DNS of droplet evaporation and combustion in a swirling combustor

By K. Luo, O. Desjardins† AND H. Pitsch

1. Motivation and objectives

Turbulent multi-phase combustion is encountered in a number of engineering applications, such as internal combustion engines and gas-turbine aircraft engines. Therefore, the ability to perform accurate numerical simulations of these systems is of paramount importance to improve their design and efficiency. However, the underlying physics of spray combustion are extremely complicated. The liquid phase undergoes primary and secondary atomization. The resulting droplets are subject to evaporation, condensation, further breakup, or collision and coalescence with other droplets. The resulting vapor in the gas phase undergoes turbulent mixing, supplying the flame with unburned evaporated fuel. These concurrent processes of liquid-phase dynamics and evaporation, turbulence and combustion interact and strongly affect each other. Much pioneering effort has been dedicated to DNS of 2-D spray combustion in simple configurations and many interesting features have been obtained (Miller & Bellan 1999; Reveillon 2007). To gain a better understanding of the interactions between combustion and evaporation in a more realistic case, DNS of a 3-D swirling n-heptane spray flame is presented here. The structure characteristics of the spray flame are analyzed. Both premixed and diffusion flames are observed. The simulation is also used to extract data relevant to combustion modeling for future research.

2. Mathematical model

2.1. *Governing equations*

The gas phase is described using the variable density, low-Mach number Navier-Stokes equations. The influence of the spray appears in terms of a mass source term $\dot{S}_m$ in the continuity equation and a momentum source term $\dot{S}_i$ in the momentum equations. These equations read

$$\frac{\partial \rho}{\partial t} + \frac{\partial \rho u_i}{\partial x_i} = \dot{S}_m, \tag{2.1}$$

and

$$\frac{\partial \rho u_i}{\partial t} + \frac{\partial \rho u_i u_j}{\partial x_j} = -\frac{\partial p}{\partial x_i} + \frac{\partial \sigma_{ij}}{\partial x_j} + \dot{S}_i, \tag{2.2}$$

where

$$\sigma_{ij} = \mu \left(\frac{\partial u_i}{\partial x_j} + \frac{\partial u_j}{\partial x_i} \right) - \frac{2}{3} \mu \frac{\partial u_k}{\partial x_k} \delta_{ij}. \tag{2.3}$$

Three additional scalar transport equations corresponding to the mass fractions of fuel (F), oxidizer (O), and products (P) are solved. They include chemical source terms $\dot{\omega}_i$,

† Current Address: Department of Mechanical Engineering, College of Engineering and Applied Science,University of Colorado at Boulder

$i \in \{F, O, P\}$, and the fuel mass fraction equation contains the same spray evaporation mass source term that appears in the continuity equation, $\dot{S}_m$:

$$\frac{\partial \rho Y_F}{\partial t} + \frac{\partial \rho Y_F u_j}{\partial x_j} = \frac{\partial}{\partial x_j}\left(\rho D_F \frac{\partial Y_F}{\partial x_j}\right) + \dot{\omega}_F + \dot{S}_m, \tag{2.4}$$

$$\frac{\partial \rho Y_O}{\partial t} + \frac{\partial \rho Y_O u_j}{\partial x_j} = \frac{\partial}{\partial x_j}\left(\rho D_O \frac{\partial Y_O}{\partial x_j}\right) + \dot{\omega}_O, \tag{2.5}$$

and

$$\frac{\partial \rho Y_P}{\partial t} + \frac{\partial \rho Y_P u_j}{\partial x_j} = \frac{\partial}{\partial x_j}\left(\rho D_P \frac{\partial Y_P}{\partial x_j}\right) + \dot{\omega}_P. \tag{2.6}$$

Finally, a transport equation is solved for the temperature of the gas phase:

$$\frac{\partial \rho c_p T}{\partial t} + \frac{\partial \rho c_p T u_j}{\partial x_j} = \frac{\partial}{\partial x_j}\left(\lambda \frac{\partial T}{\partial x_j}\right) + \dot{\omega}_T + \dot{S}_T, \tag{2.7}$$

where $\dot{S}_T$ is the energy exchange with the droplets, and $\dot{\omega}_T$ is the rate of the heat release in the combustion process.

Dispersed particles are known to follow the Basset-Boussinesq-Oseen equations. However, it is assumed here that the drag force dominates the droplet motion. The Basset history term, the added mass effect and the unsteady drag effect are neglected, as all these terms are small for large density ratios. Collisions and coalescence are neglected, since the volumetric loading of drops is small. As a result, the equations for the droplet position $x_{d,i}$ and velocity $u_{d,i}$ are written as (Maxey & Riley 1983):

$$\frac{dx_{d,i}}{dt} = u_{d,i}, \tag{2.8}$$

and

$$\frac{du_{d,i}}{dt} = \frac{f_1}{\tau_d}\left(u_i - u_{d,i}\right) + g_i. \tag{2.9}$$

In Eq. (2.9), g_i is the gravitational force, τ_d is the particle time constant and f_1 is an empirical correction to the Stokes drag law for larger droplet Reynolds numbers.

2.2. *Droplet evaporation model*

To study evaporation-combustion interactions and relevant modeling issues, accurate descriptions of both droplet evaporation and vapor combustion subprocesses are crucial. Regarding liquid droplet evaporation, a variety of models exist and can be divided into six groups in terms of complexity (Sirignano 1999; Sazhin *et al.* 2006). In the present study, considering both the complexity and accuracy, we use the infinite thermal conductivity model with some corrections, and assume that there is no temperature gradient inside droplets. The validation of the adopted model will be presented in the following. The heating and evaporation of single-component droplets can be expressed in terms of the mass-transfer number defined by:

$$B_M = \frac{Y_F^{\mathrm{surf}} - Y_F}{1 - Y_F^{\mathrm{surf}}}, \tag{2.10}$$

where Y_F is the mass fraction of the fuel at the droplet position, and Y_F^{surf} is the mass fraction of the fuel at the surface of the droplet, obtained from the Clausius-Clapeyron saturation law (Cengel & Boles 2005) by assuming local equilibrium between the droplet

and the ambient gas. The following equations for droplet temperature T_d and mass m_d are then obtained:

$$\frac{dT_d}{dt} = \frac{\mathrm{Nu}}{3\mathrm{Pr}} \frac{c_{p,m}}{c_L} \frac{f_2}{\tau_d} (T_g - T_d) + \frac{\dot{m}_d L_V}{m_d c_L}, \tag{2.11}$$

and

$$\frac{dm_d}{dt} = \dot{m}_d = -\frac{\mathrm{Sh}}{3\mathrm{Sc}} \frac{m_d}{\tau_d} \ln(1 + B_M), \tag{2.12}$$

where Nu and Sh are the corrected Nusselt and Sherwood numbers to account for the convection effect on evaporation, and f_2 is a correction for the effect of droplet evaporation on droplet heating. This correction has been proven to be important (Miller *et al.* 1998). Another important issue to droplet evaporation modeling is the specification of the physical properties used in the above equations. Several previous studies have shown that evaporation-rate predictions are sensitive to the choice of property values of gas and vapor (Kassoy & Williams 1968; Law & Law 1976). The general approach is to define a reference temperature and a vapor mass fraction, which are used to evaluate both the gas and vapor properties. Given the vapor and gas properties evaluated at the reference temperature, the physical properties for the mixture can be calculated using the reference mass fraction weighted averaging procedure. However, this procedure is generally needed at each time step and can significantly increase computational cost in spray combustion where many droplets are usually involved. To avoid this, we follow Miller *et al.* (1998) to evaluate physical properties based on an estimated wet bulb temperature, which has been demonstrated to be an efficient approach. In this way, physical properties only need to be evaluated in the beginning of the simulations. Finally, the liquid droplet density ρ_L, heat capacity c_L and latent heat of vaporization L_V are assumed constant.

2.3. *Combustion model*

To study the actual combustion process, the detailed chemistry is generally preferable. Nevertheless, it is very computationally expensive. In the present study, we focus on the global characteristics of spray combustion with an emphasis of the effect of combustion and evaporation. The combustion process is therefore chosen to be represented by a one-step global reaction model of n-heptane. The choice is motivated by the low spatial resolution requirements of such a model, in comparison to multiple-steps models. However, in order to retain as much as possible of the physical processes found in spray combustion, the approach proposed recently by Fernandez-Tarrazo *et al.* (2006) will be followed, where the coefficients of the Arrhenius law are fitted in order to accurately reproduce the burning velocity for the problem of interest for both lean and rich fuel/air ratios. Such a methodology has also been shown to be able to reproduce the rate of strain at extinction.

The chemical source terms $\dot{\omega}_F$, $\dot{\omega}_O$, $\dot{\omega}_P$, and $\dot{\omega}_T$ in Eqs. 2.4, 2.5, 2.6, and 2.7 are obtained from the following one-step irreversible reaction of n-heptane:

$$\upsilon_F F + \upsilon_O O \rightarrow \upsilon_P P + Q, \tag{2.13}$$

where the stoichiometric coefficients υ_i are taken from the global n-heptane oxidation reaction $\mathrm{C_7H_{16}} + 11\mathrm{O_2} \rightarrow 7\mathrm{CO_2} + 8\mathrm{H_2O}$, and Q is the heat release.

3. Flow configuration and numerical schemes

The flow configuration for a swirling stabilized spray flame is shown in Fig. 1. The geometry is based on some experimental configuration, but has been scaled down sig-

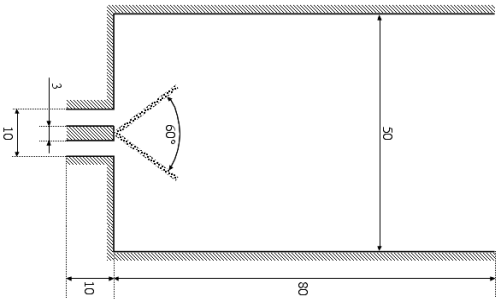

FIGURE 1. Schematics of the swirling combustor (all dimensions are given in mm).

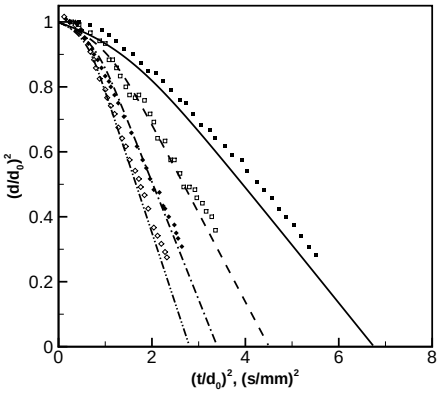

FIGURE 2. Time variations of normalized squared droplet diameter of n-heptane (—··— Tg=741 K, predicted; ◊ Tg=741 K, exp.; —·— Tg=648 K, predicted; ♦ Tg=648 K, exp.; – – – – Tg=555 K, predicted; □ Tg=555 K, exp.; ——— Tg=471 K, predicted; ■ Tg=471 K, exp.).

nificantly to allow for direct simulation of all scales. Swirling air is injected through an annular pipe of inner diameter $D_{\text{in}} = 3$ mm and outer diameter $D_{\text{out}} = 10$ mm, with a mean axial velocity $U_{\text{inj}} = 3$ m/s and a mean swirl velocity $W_{\text{inj}} = 3$ m/s. The combustion chamber is 50 mm wide and 80 mm long, while the injection pipe is 10 mm long. The Reynolds number, based on the bulk inflow velocity and outer diameter of the pipe, is approximately 2000. The n-heptane droplets are introduced from the tip of the central wall region inside the annular pipe, through a hole of diameter 0.25 mm. Initially, the droplet axial and radial velocities are set as 13 m/s and 7.5 m/s, respectively, with the droplet mass flow rate of 1.214×10^{-5} kg/s and a temperature of 300 K. The spray cone angle is 60^0 and the group combustion number $G = 5N^{2/3}/S \approx 100$, which means that the present droplet combustion is expected to be in the external group combustion regime (Chui & Liu 1977). To generate turbulent inflow conditions for the swirling air, a separate DNS of a pipe flow is conducted, and the data at some axial position are saved and used as the inflow. The estimated Kolmogorov length scale is approximately 2.47×10^{-4} m. For DNS studies of spray combustion, there are various limits to the grid size. The grid size has to be small enough to resolve both the Kolmogorov length scale and the flame reaction zone thickness. But the grid size has to be much larger than the droplet size if the point-source assumption is to be used for the droplets. Typically, the reaction zone thickness of n-heptanes flame is on the order of 2×10^{-5} m, and the droplet size ranges from 1×10^{-5} m to 1×10^{-4} m. This restricts the application scope of DNS. In the present study, a one-step global reaction is used, which requires much less resolution than multi-step chemistry, since the thin radical layers do not need to be resolved. The grid for the preliminary simulations presented here is composed of 384 grid points along the axial direction x, 192 grid points along the radial direction y and 128 grid points along the swirling direction θ. To capture the important structures as much as possible, the mesh is non-uniform. In the regions of recirculation, strong shear and near wall, the mesh is finer than in other regions. The largest mean grid scale is approximately 2.6×10^{-4} m, which is on the order of the estimated Kolmogorov length scale

and the flame thickness. The flow is periodic in the swirling direction, and no-slip wall boundary conditions are used in the radial direction. The downstream outflow condition is obtained by solving a convection equation, allowing for a smooth exit of all structures without perturbing the rest of the flow significantly. First, hot air with a temperature of 900 K is injected to trigger combustion. Then the air temperature is decreased to 300 K. The data are stored when the flame becomes approximately stable.

The low-Mach number Navier-Stokes equations are discretized using a fourth order in space, second order in time, staggered scheme (Desjardins *et al.* 2008). This scheme is derived from Morinishi *et al.* (2004) and has excellent conservation properties. Mass and momentum are exactly conserved even on non-equidistant grids. A fractional-step approach is used for the time integration. The spray is described using a Lagrangian solver that uses a fourth order Runge-Kutta fully coupled time integration of the droplet equations. The information from the gas phase is interpolated at the droplet positions using a tri-linear interpolation. The transfer of source terms back to the gas phase from the spray is based on the particle-in-cell (PIC) approach. Adaptive time-stepping is required to allow for an accurate integration of the equations when the drops become very small without significant increase in the computational cost. Once the droplet diameter falls below 1 micrometer, it will be removed from the calculation, and the rest of its mass, momentum and energy will be transferred to the gas phase. This approach seems consistent since the influence of such very small droplets becomes negligible.

4. Model validation

First, the heating and evaporation model for a single liquid droplet is validated against available experimental data. Although some validation and comparative analysis of droplet evaporation models have been presented in previous studies (Miller *et al.* 1998; Sazhin 2006), most of them are conducted in zero-dimensional cases and the variation of gas temperature at the droplet position is either neglected or averaged. However, in practical 3-D unsteady simulations, the ambient gas temperature and vapor mass fraction are not constant, but vary in both time and space. In this case, the gas temperature T_g in Eq. (2.11) which is used to calculate inter-phase heat and mass transfers, becomes a key issue for transient heating and evaporation of the droplet. The local gas temperature obtained by interpolation from surrounding grid points appears to be a natural choice. However, since the models for calculating heat transfer between droplets and gas are typically formulated in terms of far-field ambient gas temperature or mainstream gas temperature, the employed local gas temperature must approximately satisfy this condition. Evidently, the local gas temperature is strongly dependent on the grid size and affected by the cooling effect from evaporation, which imposes another condition for droplet evaporation prediction, but has not been addressed in previous studies. In the present study, the heating and evaporation model of a single droplet is validated in 3-D simulations initially based on the constant ambient gas temperature. Then, the grid-size dependence is discussed when the local gas temperature is used.

Figure 2 shows the comparisons of the predicted time variations of normalized squared droplet diameter of n-heptane with those obtained in the experiments (Nomura *et al.* 1996). The predicted results agree well with the experimental data, especially for the higher temperature cases. Note that we use the constant ambient temperature and neglect the variation of the local gas temperature. In this case, the effect of the grid size on droplet evaporation may be negligible, as shown in Fig. 3. However, in practical sim-

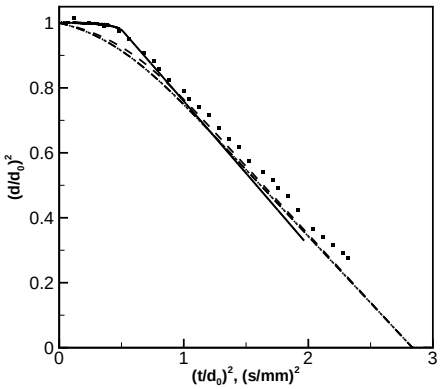

FIGURE 3. Time variation of normalized squared droplet diameter of n-heptane at P=1atm and an ambient temperature of 741 K (■, exp.;——— $\triangle/d_0$=0.14; – – – – $\triangle/d_0$=1.4; —·— $\triangle/d_0$=14; —··— $\triangle/d_0$=71). In the calculations, constant ambient temperature and different grid sizes $\triangle$ are used.

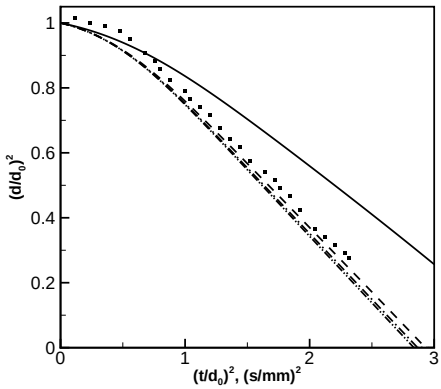

FIGURE 4. Time variations of normalized squared droplet diameter of n-heptane under the conditions of P=1atm at an ambient temperature of 741K (■, exp.;——— $\triangle/d_0$=1.4; – – – – $\triangle/d_0$=7.1; —·— $\triangle/d_0$=14; —··— $\triangle/d_0$=71). In the calculations, the local gas temperature and different grid sizes $\triangle$ are used.

ulations, the ambient temperature is not constant, and a more local gas temperature has to be used, which is dependent on the ratio of the cell size to the droplet diameter. Figure 4 shows that when the grid size is on the order of or larger than 10 times the droplet diameter, using the local gas temperature can yield results consistent with the experimental data. Otherwise, the predicted droplet evaporation will significantly deviate from the experiment data. This would indicate that the cooling effect resulting from evaporation can only influence the gas temperature within a range of about 10 times the droplet diameter, which is consistent with the recent analytical solutions of the heat conduction equation obtained by Sazhin *et al.* (2007). This suggests that the grid size has to be at least 10 times the droplet diameter if the local gas temperature is used for 3-D evaporation prediction. Thus, the droplet diameter used in the present spray study is restricted to less than 2.6×10^{-5} m. Hence, the initial droplet diameter is set as 2×10^{-5} m to ensure the accuracy of evaporation prediction, which is important for studying evaporation-combustion interactions. Although the resulting Weber number of 146 and Ohnesorge number of 0.237 indicate the droplets are in the shear break-up regime, the droplet break-up is neglected in the present study.

The validation of the evaporation model is also extended to other fuels, such as decane and hexane. Figure 5 shows the time variations of droplet diameter squared and the droplet temperature for decane. The experimental data reported by Wong & Lin (1992) are also plotted. The comparison of temporal evolution of hexane droplet diameter squared between predicted results and experimental data (Downing 1966) is presented in Fig. 6. The predicted results based on the model are generally in good agreement with available experimental data, which also validates the evaporation model used in the present study.

When combustion of the evaporated vapor happens, the situation becomes more complicated. The cooling effect from evaporation decreases the gas temperature, but at the same time it is increased by heat release from combustion. Although some experimental

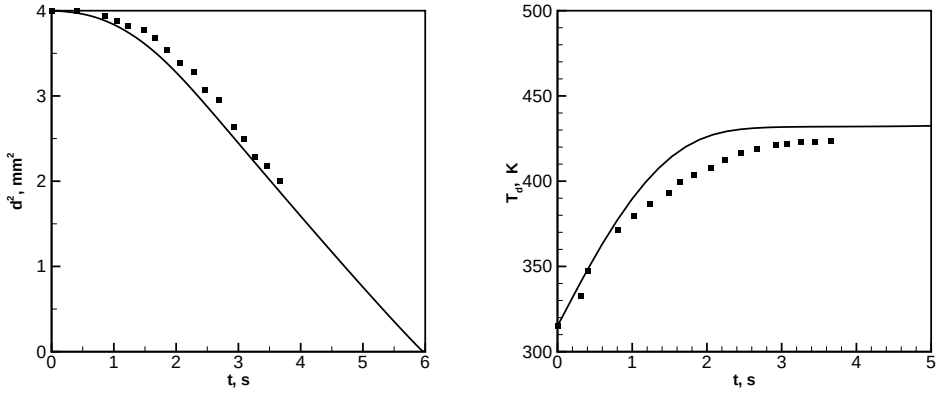

FIGURE 5. Time variation of the droplet diameter squared (left) and the droplet temperature (right) for decane (——— predicted; ■ exp.). The experimental data are from Wong & Lin (1992), and the conditions are: T_g=1000K, T_d=315K, d_0=2mm and $\mathrm{Re}_{d,0}$=17.

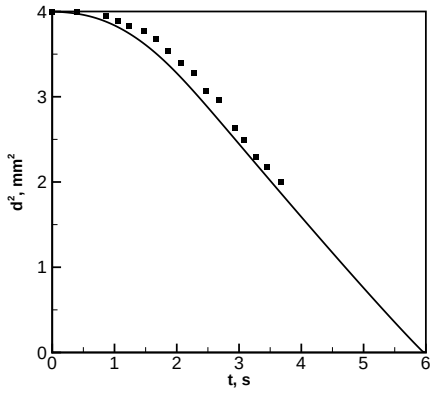

FIGURE 6. Time variation of the droplet diameter squared for hexane (——— predicted; ■ exp.). The experimental results are from Downing (1966) and the conditions are: T_g=437, $\mathrm{T}_{d,0}$=281K, d_0=1.76 mm and $\mathrm{Re}_{d,0}$=110.

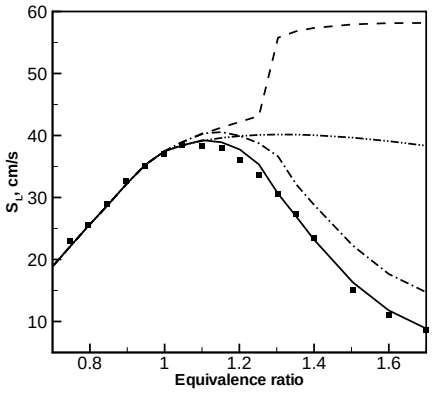

FIGURE 7. Experimental and predicted laminar flame speed for n-heptane (■ exp.(Davis & Law 1998);——— Variable heat release Q and activation temperature T_a;—·— Variable Q and constant T_a; —··— Constant Q and constant T_a; – – – Constant Q and constant T_a).

data on single droplet combustion in microgravity conditions are available (Marchese & Dryer 1997), the direct validation of the model is beyond the scope of the present study. In almost all experiments, the droplet size is on the order of 1×10^{-3} m. According to the previous discussion, the mesh spacing has to be about ten times larger than 1×10^{-3} m in the context of point-particle assumption. But the grid size also has to be smaller than the flame thickness (typically 2×10^{-4} m) to resolve the flame. This conflict restricts the application of the current point-based Lagrangian particle-tracking method.

As an alternative, we attempt to validate the combustion model by comparing the predicted laminar flame speed with related experimental data (Davis & Law 1998), shown in Fig. 7. Along with the experimental data, the predicted results based on the global

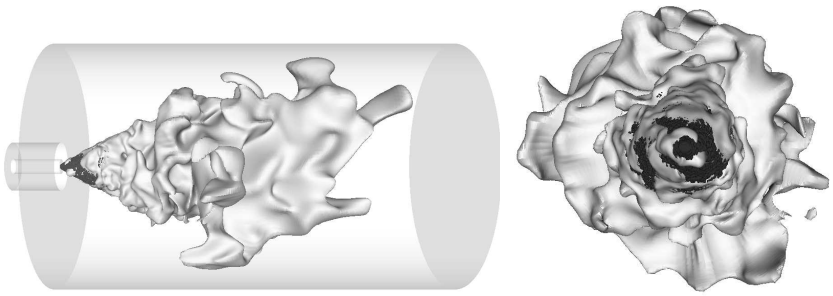

FIGURE 8. Isosurfaces of stoichiometric mixture fraction and distribution of droplets (black points) at t=0.442 s. Left: front view; right: side view.

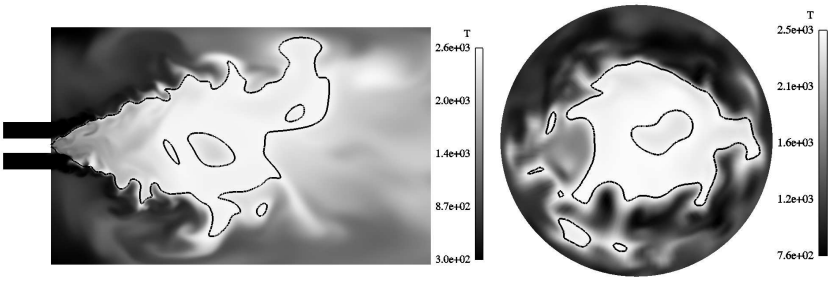

FIGURE 9. Contours of temperature at t=0.442 s in the planes of θ=0 (left) and x=3e-2 m (right). The black lines indicate the locations with stoichiometric mixture fraction.

one-step combustion model with variable/constant heat release and variable/constant activation temperature are provided. It is observed that the combustion model proposed by Fernandez-Tarrazo *et al.* (2006) with adaptive heat release and adaptive activation temperature can accurately reproduce the laminar flame-burning velocity, which is important to combustion modeling. With these two adaptive parameters in the model, the over-prediction of laminar flame speed in the fuel-rich side that often occurs in traditional one-step combustion model is avoided.

5. Results and discussions

5.1. *Instantaneous results*

Figure 8 presents the instantaneous isosurfaces of stoichiometric mixture fraction and droplet distribution at the time t=0.442 s. The combustion of droplets happens in external group combustion mode and the flame front is stabilized by the spray cone. The flame surface appears to be very thin and wrinkled. This provides some clues for the modeling study in the next step. The instantaneous contours of temperature at the same time are shown in Fig. 9, where the black lines denote the locations with stoichiometric mixture fraction. The temperature in the spray cone near the nozzle is lower than further downstream locations due to the cooling effect created by droplet evaporation. There also exist some isolated pocket regions surrounded by the stoichiometric lines, indicating local pocket combustion because of local fuel source of droplet evaporation.

To further examine the spray flame structures, a normalized flame index is used (Domingo *et al.* 2005). Based on this flame index, we can identify different combustion modes. For a fully premixed flame, the flame index is unity and for diffusion flames, the

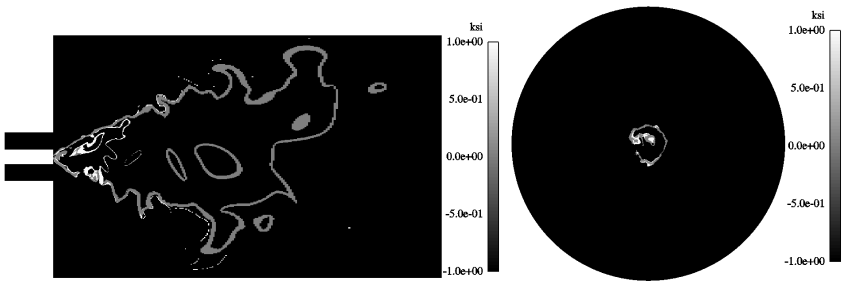

FIGURE 10. Instantaneous contours of flame index at the time t=0.442 s in the planes of θ=0 (left) and $x = 5 \times 10^{-3}$ m that is close to the spray nozzle (right).

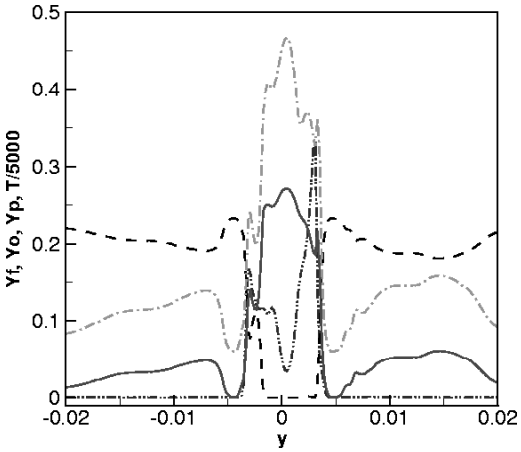

FIGURE 11. Instantaneous distribution of species and temperature along the line of $\{x = 5 \times 10^{-3}\text{m}, \theta = 0.0\text{m}\}$ at the time t=0.408 s (—·—·— Yf; – – – – Yo; ——— Yp; —·— T/5000).

flame index is zero. It is observed that in the fuel-rich side just behind the spray cone, premixed flames occur and some isolated pocket flames exist as discussed earlier. But in the fuel-lean side, diffusion flames dominate. This can also be seen from the instantaneous distribution of species and temperature along the vertical line of $\{x = 5 \times 10^{-3}\text{m}, \theta = 0.0\text{m}\}$ at the time t=0.408 s, as shown in Fig. 11. At $|y| = 0.004$ m, the mass fraction of fuel reaches its maximum values at high levels of oxidizer concentration, which results in premixed combustion. Then due to lack of fuel, diffusion combustion develops outside in the region where fuel and oxidizer go to zero. As for the regions near the central line, it is found that the mass fraction of oxidizer is zero, but the product and temperature reach their peaks. This is caused by the recirculation in the core region. With higher product temperature in this recirculation region, droplets are easily evaporated and can provide stable combustion.

5.2. *Averaged results*

The averaged evaporation, premixed and diffusion combustion source terms are defined as function of axial location x as below to evaluate their relative importance.

$$\overline{\dot{\omega}_i} = \frac{\iint \beta \dot{\omega}_i \, dr \, d\theta}{\iint \, dr \, d\theta} \tag{5.1}$$

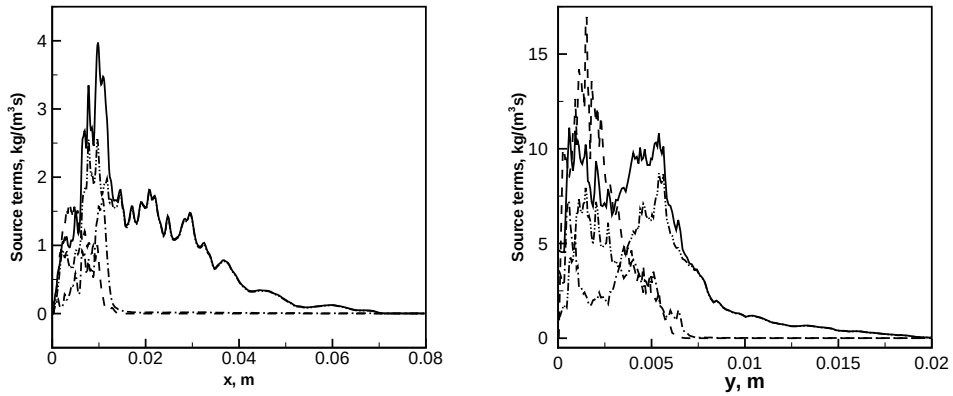

FIGURE 12. Distributions of the averaged evaporation and chemical source terms along the axis (left) and radial (right) directions (——— Chemical source term; —··— Diffusion combustion rate; —·— Premixed combustion rate; - - - - Evaporation source term).

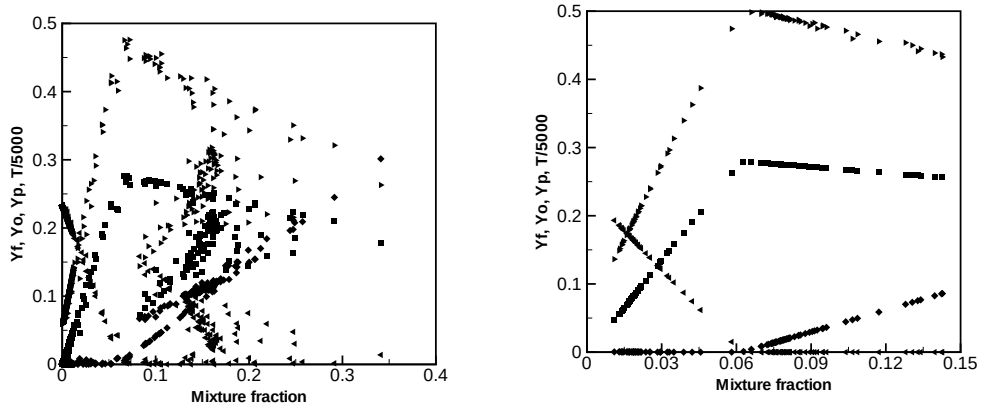

FIGURE 13. Scatter plots of species mass fraction and temperature as function of mixture fraction at different axial planes (▷ T/5000; ■ Yp; ◁ Yo; ♦ Yf). Left: $x = 2 \times 10^{-3}$ m; right: $x = 3 \times 10^{-2}$ m.

where $\dot{\omega}_i$ denote the evaporation, total burning, premixed burning and diffusion burning source terms, respectively. β is constant, set as unity for evaporation and total burning source terms, and equal to flame index for premixed burning and diffusion burning source terms. Fig. 12 presents the distributions of the averaged evaporation and chemical source terms along the axial direction. Evidently, the diffusion combustion rate is higher than the premixed counterpart. Evaporation and premixed combustion are limited to the region $0 < x < 0.012$ and $0 < |y| < 0.006$, but the diffusion flame extends beyond this. Furthermore, the overlap of evaporation and combustion regions suggests that evaporation and combustion are strongly coupled in both time and space. The above results show that spray flames are composed of weak premixed flames and strong diffusion flames. The double flame structures present challenges for spray combustion modeling. To overcome this issue, models considering both premixed and diffusion combustion need to be developed.

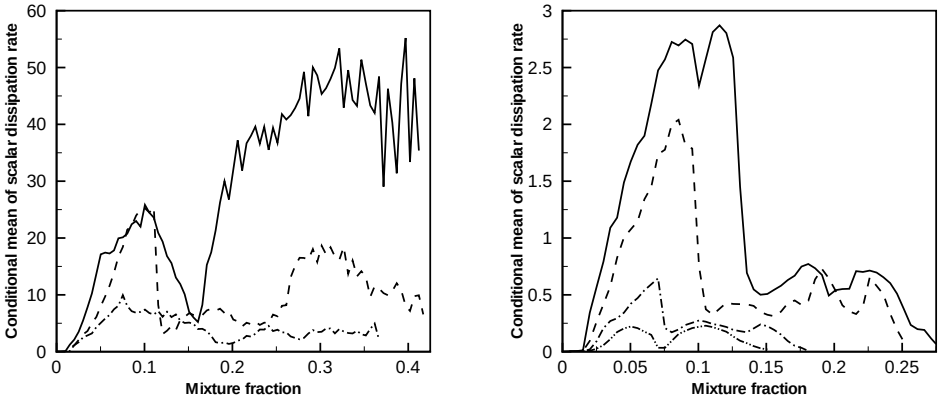

FIGURE 14. Conditional mean of the scalar dissipation rate at different axis locations. Left: upstream locations (——— x=2e-3; - - - - x=5e-3; —·— x=1e-2); right: downstream locations (——— x=1.5e-2; - - - - x=2e-2; —·— x=2.5e-2; —··— x=3e-2).

Figure 13 depicts the scatter plots of the mass fraction of species and temperature in mixture fraction space at different axial planes. In the spray region near the nozzle, the scatter significantly deviates from chemical equilibrium for all scalars. The temperature close to the nozzle shows a bi-modal behavior, which results from burning regions and non-burning rich regions with an equivalence ratio beyond the flammability limit. Again, this effect needs to be taken into account for model developments.

5.3. *Statistics of conditional means*

Most non-premixed combustion models rely on the scalar dissipation rate to describe the mixing process between fuel and oxidizer. In flamelet modeling, it is common practice to assume the shape of the conditional mean scalar dissipation rate as a function of mixture fraction. However, this assumption may not be applicable to spray combustion, as the mixing process is modified by droplet evaporation. To examine this, conditional statistics of the scalar dissipation rate are extracted from the DNS and shown in Fig. 14. The distribution of the conditional mean of the scalar dissipation rate displays bi-modal structures in mixture fraction space. The first peak is approximately of stoichiometric conditions, but the second depends on downstream location. Close to the nozzle, the conditional mean of the scalar dissipation rate increases, especially in the spray region near the nozzle. This indicates that the local droplet evaporation significantly alter the scalar dissipation rate, which needs to be accounted for in future modeling.

6. Summary and future work

DNS of droplet evaporation and combustion in a swirling combustor has been conducted. Some features of spray flames are discussed and the challenges for modeling development are highlighted here. In the next step, more relevant cases for realistic gas turbine combustors will be pursued and DNS data will be analyzed in detail. Models that can account for both premixed and diffusion flames in spray combustion will also be developed and assessed.

Acknowledgements

The authors are grateful for NASA's support of this project.

REFERENCES

Cengel, Y. A & Boles, M. A. 2005 *Thermodynamics: An Engineering Approach (5th).* McGraw-Hill Series in Mechanical Engineering. Boston: McGraw-Hill.

Chui, H. H. & Liu, T. M. 1977 Group combustion of liquid droplets. *Combust. Sci. Technol.* **17**, 127-142.

Davis, S. G. & Law, C. K. 1998 Laminar flame speeds and oxidation kinetics of iso-octane-air and n-Heptane-air flames. *Proc. Combust. Inst.* **27**, 521-527.

Desjardins, O., Blanquart, G., Balarac, G. & Pitsch, H. 2008 High order conservative finite difference scheme for variable density low Mach number turbulent flows. *J. Comp. Phys.* **227**(15), 7125-7159.

Domingo, P., Vervisch, L. & Reveillon, J. 2005 DNS analysis of partially premixed combustion in spray and gaseous turbulent flame-bases stabilized in hot air. *Combust. Flame* **140**(3), 172-195.

Downing, C. G. 1966 The evaporation of drops of pure liquids at elevated temperatures: rates of evaporation and wet-bulb temperatures. *AIChE J.* **12**(4), 760-766. Miller1999

Fernandez-Tarrazo, E., Sanchez, A. L., Linan, A. & Williams, F. A. 2006 A simple one-step chemistry model for partially premixed hydrocarbon combustion. *Combust. Sci. Technol.* **147**(1-2), 32-38.

Kassoy, D. R. & Williams, F. A. 1968 Variable property effects on liquid droplet combustion. *AIAA J.* **6**(10), 1961-1965.

Law, C. K. & Law, H. K. 1976 Quasi-steady diffusion flame theory with variable specifc heats and transport coefficients. *Combust. Sci. Technol.* **12**, 207-216.

Marchese, A. J. & Dryer, F. L. 1997 The effect of non-luminous thermal radiation in microgravity droplet combustion. *Combust. Sci. Technol.* **124**, 371402.

Maxey, M. R. & Riley J. J. 1983 Equation of motion for a small rigid sphere in a non-uniform flow. *Phys. Fluids* **26**(4), 883-889.

Miller, R. S., Harstad, K. & Bellan, J. 1998 Evaluation of equilibrium and non-equilibrium evaporation models for many-droplet gas-liquid flow simulations. *Int. J. Multiphase Flow* **24**, 1025-1055.

Miller, R. S. & Bellan, J. 1999 Diret numerical simulation of a confined three-dimensional gas mixing layr with one evaporating hydrocarbon-droplet-laden stream. *J. Fluid Mech.* **384**, 293-338.

Morinishi, Y., Vasilyev, O. V. & Takeshi, O. 2004 Fully conservative finite difference scheme in cylindrical coordinates for incompressible flow simulations. *J. Comp. Phys.* **197**(2), 686-710.

Nomura, H., Ujiie, Y., Rath, H. J., Sato, J. & Kono, M. 1996 Experimental study on high-pressure droplet evaporation using microgravity conditions. *Proc. Combust. Instit.* **26**, 1267-1273.

Reveillon J. 2007 Direct numerical simulation of sprays: turbulent dispersion, evaporation and combustion. *In Multiphase Reacting Flows: Modeling and Simulation* **492**, 229-269. New York: Springer Vienna.

Sazhin, S. S. 2006 Advanced models of fuel droplet heating and evaporation. *Progress in Energy and Combustion Science* **32**, 162-214.

Sazhin, S. S., Kristyadi, T., Abdelghaffar, W.A. & Heikal, M. R. 2006 Models for fuel droplet heating and evaporation: Comparative analysis. *Fuel* **85**(12-13), 1613-1630.

Sazhin, S. S., Krutitskii, P. A., Martynov, S. B., Mason, D., Heikal, M. R. & Sazhina, E. M. 2007 Transient heating of a semitransparent spherical body. *Int. J. Thermal Science* **46**(5), 444-457.

Sirignano, W. A. 1999 Fluid Dynamics and Transport of Droplets and Sprays. United Kingdom: Cambridge University Press.

Wong, S. C. & Lin, A. R. 1992 Internal temperature distributions of droplets vaporizing in high-temperature convective flows. *J. Fluid Mech.* **237**, 671-687.